ELSEVIER

Polymer 43 (2002) 5147–5155

polymer

www.elsevier.com/locate/polymer

Chemometric solid-state ^{13}C NMR analysis of morphology and dynamics in irradiated crosslinked polyolefin cable insulation

D.J. Harris*, M.K. Alam

Sandia National Laboratories, Albuquerque, NM 87185-1411, USA

Received 28 May 2002; accepted 31 May 2002

Abstract

The relative concentrations and carbon spin–lattice relaxation constants ($T_{1,C}$) of the amorphous, intermediate, and crystalline phases of unaged crosslinked polyolefin cable insulation (ultimate elongation, $e = 310\%$), ^{60}Co γ-irradiated ($e = 22\%$), and irradiated + annealed ($e = 220\%$) samples were determined by chemometric analyses of directly polarized solid-state ^{13}C NMR spectra. The $T_{1,C}$ relaxation curves of the intermediate and amorphous components were found to be mono-exponential. The intermediate component contains 23 ± 5% of the CH_2 segments in the unaged sample and has an $T_{1,C}$ relaxation constant of 1.4 ± 0.3 s. γ-Irradiation caused a slight decrease in the amount of intermediate component to 19 ± 5% and an increase of the relaxation constant to 1.8 ± 0.3 s. The subsequent annealing of the irradiated sample resulted in an additional increase of the relaxation constant to 2.1 s and a slight loss of crystallinity. The amorphous $T_{1,C}$ relaxation constants were found to be identical in all three samples and have a value of 0.38 ± 0.03 s. At ambient temperature, the crystalline phase was found to relax via chain diffusion from the intermediate component. The rate of helical jumps was twice as fast in the irradiated and irradiated + annealed samples compared with the unaged material.

Keywords: Polyethylene; Nuclear magnetic resonance; Chemometrics

1. Introduction

Lifetime prediction for polymeric materials often rely on accelerated aging at elevated temperatures. Combined irradiation and thermal aging of several varieties of crosslinked polyolefin (XLPO) cable insulation materials showed inverse temperature behavior [1,2]. Samples subjected to radiation in the presence of oxygen at ambient temperature were shown to have lower ultimate elongation than materials irradiated at higher temperatures. The findings also discovered the 'Lazarus effect' where annealing can extend the lifetime of dead insulation. Annealing at 140 °C for 24 h allowed significant recovery of elongation for ambient temperature materials. The recovery of elongation has been reported to be as large as 200% for certain samples. The values after annealing matches those for materials irradiated at higher temperatures.

Understanding the structure–property relationships that govern the degradation behavior of the cable insulation is an important goal for designing better materials. Several techniques had shown small material changes during the annealing processes. Gel content decreased 7% due to radiation but increased 17% after annealing. Differential scanning calorimetry (DSC) showed little loss of crystallinity during irradiation but extensive loss of the 122 °C melting peak after annealing. The thermograms were complex and exhibited broad melting behavior for all samples. The change of melting enthalpy after annealing corresponds to an absolute 3% decrease in crystallinity. These modest differences cannot be used to explain the very large loss and subsequent recovery of mechanical properties.

This paper investigates in further depth the structure–property relationships that govern the Lazarus effect. The mechanical properties of semicrystalline polymers have been shown to be dependent on the crystallite thickness, and the relative abundances of amorphous and interfacial regions [3,4]. Previous studies have suggested that radiation may selectively damage polyolefins at the surfaces and defects of crystallites, or break tie chains connecting crystalline lamellae [5,6]. One of the most powerful techniques to quantitatively determine both the dynamics and morphology of polyethylene is solid-state nuclear magnetic resonance (NMR) spectroscopy. The chemical

* Corresponding author. Address: FM Global Research, 1151 Boston-Providence Turnpike, Norwood, MA 02062, USA. Tel.: +1-781-769-8184.
E-mail address: wolfgang@alum.mit.edu (D.J. Harris).

0032-3861/01/$ - see front matter
PII: S0032-3861(02)00368-3

shifts of peaks in ^{13}C spectra have been assigned to morphological domains [7,8] on the basis of γ-*gauche* [9] and packing effects. The all-*trans* orthorhombic crystalline component has an isotropic chemical shift of $\delta = 32.8$ ppm [10,11] while *gauche*-containing amorphous segments have upfield chemical shifts [7]. The all-*trans* monoclinic crystalline phase has a resonance shifted downfield to $\delta =$ 34.3 ppm due to packing effects [8].

In addition to amorphous and crystalline phases, recent research has postulated the presence of an intermediate 'phase' that is sometimes assigned to be interfacial chains [12,13]. The intermediate component is of great interest to understanding the mechanical properties and physics of semicrystalline polymers. Despite the importance, no conclusive evidence has been presented to determine if the intermediate component is a discrete phase or merely a gradient of properties at the crystalline/amorphous boundary. If the latter possibility were true, quantification of the component would be technique and interpretation dependent. Several methods have been utilized to analyze the intermediate component. Deconvolution of lineshapes in Raman spectroscopy has suggested that approximately 20% of the segments may be in the intermediate regions [14]. Both ^{1}H and ^{13}C solid-state NMR methods have also been used to examine the intermediate components in polyethylene [8,15–23]. However, quantitative analysis often requires assumption of lineshape or T_1 relaxation behavior.

This paper applies chemometric analysis to the ^{13}C NMR to obtain model-independent information about both dynamics and morphology in XLPO materials. Chemometrics refers to application of statistical and mathematical methods to extract chemically relevant information from data produced in chemical experiments [24]. The chemometric method that was utilized here for analyzing polyethylene is unique because it requires no assumption of either lineshapes or relaxation constants. Other chemometric studies have shown versatility in determining lineshapes and quantifying component concentrations in complex ^{1}H [25–27], ^{13}C [28–30], ^{17}O [24,31], and ^{31}P [32] NMR spectra. Typical NMR experiments incorporating chemometrics acquire an array of spectra with incremented delays. The relaxation constants and lineshapes of the pure components can then be mathematically determined using a variety of methods including multivariate curve resolution (MCR) [33], component resolved NMR (CORE) [34,35], and the direct exponential curve resolution algorithm (DECRA) [24], the techniques used in this paper. For polyethylene, the $T_{1,C}$ relaxation constants extracted by DECRA are related to the chain dynamics [36] while the chemical shift is determined by γ-*gauche* [9] and packing effects. The chemometric analysis was supplemented with additional direct-polarization DP/MAS and $T_{1,C}$-filtered [37] crosspolarization (CP/MAS) ^{13}C NMR experiments to provide an overview of components and relaxation constants. Comparisons between unaged, irradiated, and irradiated + annealed XLPO materials are presented in this paper.

2. Experimental

2.1. XLPO cable insulation

The material used in these experiments is commercial polyethylene-*co*-vinylacetate crosslinked cable insulation without the conductor core (sample A of Ref. [2]). The material has been characterized previously [1] and was shown to contain flame retardants and TiO_2. The initial gel content, determined by *p*-xylene extraction, was reported to be 57%. Unaged material was placed in a water-tight can and subjected to radiation in flowing air for 632 d in an underwater ^{60}Co aging facility. The dose rate was 1.5 krad/h and the total dose was 23.1 Mrad. The ultimate elongation decreased from $e = 310$ to 22% due to the irradiation. Annealing was performed in a convection oven at 140 °C for 24 h. The elongation after annealing is $e = 220\%$ [2].

2.2. NMR spectroscopy

The solid-state NMR experiments were performed on a Bruker AMX400 instrument operating at frequencies of 100.61 and 400.16 MHz for ^{13}C and ^{1}H, respectively. A 4 mm broad band magic-angle spinning (MAS) probe was used with a rotor spin rate of 10 kHz. Spinning side bands are small, but significant at this frequency and were included in the analysis of relative concentrations. Typical ^{13}C $\pi/2$ pulse lengths were 4.0 μs. All ^{13}C pulse sequences employed Hahn-echoes to minimize baseline distortion and 93 kHz TPPM ^{1}H decoupling [38]. To suppress nuclear Overhauser effects (NOE) that cause excess ^{13}C magnetization recovery during short recycle delay experiments, the direct-polarization (DP/MAS) ^{13}C spectra used 5 s delays to fully relax the ^{1}H magnetization and then, prior to the effective recycle delay, destroyed the partially recovered ^{13}C magnetization using a train of eight $\pi/2$ pulses separated by 5 ms dephasing delays. The total recycle delay is thus 5 s longer than the effective delay.

Thirty DP/MAS spectra were obtained for each sample with effective recycle delays linearly spaced between 0.1 and 3.0 s. The dwell time used in each spectrum was 25 μs and the number of points was 2048. An automation program minimized irreproducibility by looping 20 times through the set of experiments, adding 64 more scans to each data set every cycle. The total experiment time was approximately 55 h for each sample. Chemical shifts were referenced to the orthorhombic crystalline peak ($\delta = 32.8$ ppm).

The monoclinic and orthorhombic phases were quantified from ^{13}C DP/MAS and $T_{1,C}$-filtered crosspolarization (CP/MAS) experiments [15,22,23] with parameters similar to those described above. DP/MAS spectra with 10 and 2000 s recycle delays determined the amorphous +

intermediate, and crystalline intensities, respectively. A 10 s $T_{1,C}$-filtered CP/MAS spectrum allowed determination of the relative ratio of orthorhombic and monoclinic crystalline phases. The CP contact-time was 0.5 ms for all applicable experiments.

^{1}H spin diffusion experiments [19,36,39–41] detected via ^{13}C CP were performed to determine the domain sizes in the samples. After a $\pi/2$ excitation pulse, the magnetization of the rigid (crystalline) ^{1}H nuclei were suppressed by a 17 μs delay. Afterwards, the magnetization was stored in the $\pm z$ direction and allowed to diffuse during a variable mixing period with a duration ranging from 0.1 to 256 ms. Following return of magnetization to the transverse plane, a 0.5 ms CP contact-time transferred magnetization to the observed ^{13}C nuclei. $T_{1,C}$-filter lengths of 0.001, 1, and 10 s were used to selectively suppress magnetization of components. When compared to DP/MAS and CP/MAS, ^{13}C experiments allowed conversion of the measured signal intensities into relative abundances of the phases. The areas were corrected for $T_{1,H}$ decay during the mixing time [36,42].

2.3. Chemometrics

The unprocessed free-induction decay signals of the DP/MAS spectra were transferred to a PC and then Fourier transformed using matNMR (http://www.nmr.ethz.ch/matnmr/). The spectra were phased prior to chemometric analysis. The number of points for each processed spectrum was reduced to 300 for analysis of the spectral region from $\delta = +52$ to -6 ppm. Only the real components of the spectra were used.

The DECRA algorithm was utilized to extract pure components and their concentration profiles from the spectral $T_{1,C}$ decay signals. The method utilizes the generalized rank annihilation method (GRAM), and requires two data sets, (**A** and **B**), that are proportional to each other (Eqs. (1) and (2))

$$\mathbf{A} = \mathbf{C}\mathbf{P}^{\mathrm{T}} \tag{1}$$

$$\mathbf{B} = \mathbf{C}\alpha\mathbf{P}^{\mathrm{T}} \tag{2}$$

where **A** and **B** are data matrices of size $s \times v$, where s is the number of spectra and v is the number of real spectral data points. **C** and **P** are the concentration matrix (size $s \times n$) and the pure component spectra matrix (size $v \times n$) for n components, respectively. Superscript T refers to the transpose operation. The diagonal proportionality matrix α relates **A** to **B**.

These proportional data sets were obtained from a single spin–lattice relaxation matrix with i equally spaced time increments, τ_i. Spectra 1 through $i-1$ were used for data set **A**, and spectra 2 through i were used for data set **B**. The modulation of the spectral signal, d_{ij} can be described assuming an exponential recovery of magnetization. The amplitude modulation of component j at effective recycle delay time τ_i is defined by d_{ij}, and is of the form

$$d_{ij}(\tau_i) = [1 - \exp(-\tau_i/T_{1j})] \tag{3}$$

where T_{1j} is the spin–lattice relaxation time of component j. Successive time increments of Eq. (3) will produce data that is not proportional to previous data. A requirement for implementation of the DECRA algorithm is that proportionality exists in order to fulfill Eqs. (1) and (2). To produce a proportional set of data, the non-exponential intercept term, 1, can be subtracted from the data, or proportionality can be achieved by adding another component to the data in the form of a constant and solving for the added component, which was the method chosen for the present data.

Eqs. (1) and (2) can be used to solve spectral and concentration profiles. Rearrangement gives

$$\mathbf{C} = \mathbf{A}(\mathbf{P}^{\mathrm{T}})^{+} \tag{4}$$

$$\mathbf{C}\alpha = \mathbf{B}(\mathbf{P}^{\mathrm{T}})^{+} \tag{5}$$

where ' + ' represents the Moore–Penrose pseudo-inverse. Multiplying Eq. (4) by α and combining with Eq. (5) gives:

$$\mathbf{A}(\mathbf{P}^{\mathrm{T}})^{+}\alpha = \mathbf{B}(\mathbf{P}^{\mathrm{T}})^{+} \tag{6}$$

Assuming $\mathbf{Z} = (\mathbf{P}^{\mathrm{T}})^{+}$ yields:

$$\mathbf{A}\mathbf{Z}\alpha = \mathbf{B}\mathbf{Z} \tag{7}$$

Eq. (7) now represents a generalized eigenvector problem. The matrix **Z** can be computed using standard routines, if **A** and **B** are square. If **A** and **B** are not square, they can be projected into a common space in order to achieve an equation containing square matrices. As Windig and Antalek [43] have discussed, there are several common spaces that can be used. For the data presented here, we have chosen to use the factor space of **A**. Estimating **A** using the significant factors of singular value decomposition produces

$$\mathbf{A} = \overline{U}\overline{S}\overline{V}^{\mathrm{T}} \tag{8}$$

where the bar refers to the truncation of the matrices to the significant factors only. Substituting into Eq. (7) gives:

$$\overline{U}\overline{S}\overline{V}^{\mathrm{T}}\mathbf{Z}\alpha = \mathbf{B}\mathbf{Z} \tag{9}$$

Assuming $\mathbf{Z}^{*} = \overline{S}\overline{V}^{\mathrm{T}}\mathbf{Z}$

$$\overline{U}\overline{S}\overline{V}^{\mathrm{T}}\overline{V}\overline{S}^{-1}\mathbf{Z}^{*}\alpha = \mathbf{B}\overline{V}\overline{S}^{-1}\mathbf{Z}^{*} \tag{10}$$

which reduces to:

$$\mathbf{Z}^{*}\alpha = \overline{U}^{\mathrm{T}}\mathbf{B}\overline{V}\overline{S}^{-1}\mathbf{Z}^{*} \tag{11}$$

Eq. (11) is now in the form of the standard eigenvalue problem, and can be solved directly, since $\overline{U}^{\mathrm{T}}\mathbf{B}\overline{V}\overline{S}^{-1}$ is square. $\mathbf{Z}^{*}$ will contain the eignevectors and α will contain the eigenvalues. Pure component spectra and concentration profiles are recovered from $\mathbf{Z}^{*}$, since

$$(\mathbf{P}^{\mathrm{T}})^{+} = \overline{V}\overline{S}^{-1}\mathbf{Z}^{*} \tag{12}$$

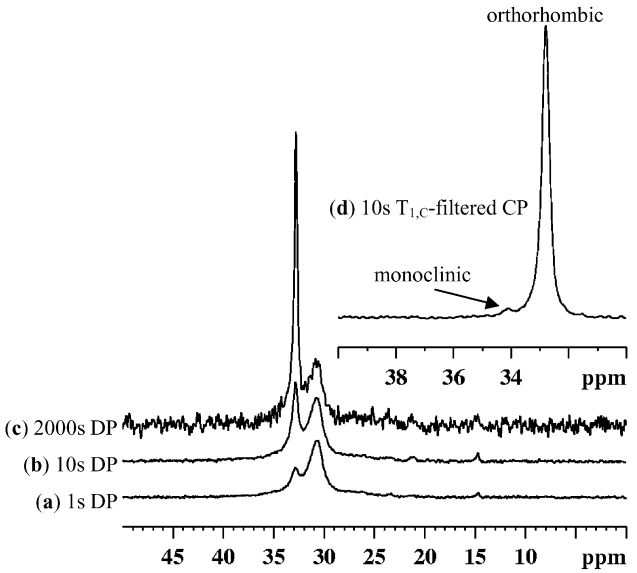

Fig. 1. Direct-polarization ^{13}C MAS NMR spectra of irradiated XLPO with effective recycle delays of (a) 1 s, (b) 10 s, (c) 2000 s. The 10 s $T_{1,C}$-filtered CP/MAS spectrum (d) shows both monoclinic and orthorhombic crystalline phases.

and

$$\mathbf{C} = \overline{U}\mathbf{Z}^{*} \tag{13}$$

3. Results and discussion

3.1. Determination of crystallinity

The ^{13}C DP/MAS and $T_{1,C}$-filtered CP/MAS NMR spectra reveal peaks arising from the amorphous, crystalline, and interfacial components. Spectra for the irradiated sample, shown in Fig. 1, differentiate the quickly relaxing broad amorphous phase ($\delta = 30.7$ ppm), the intermediate component ($\delta = 32.9$ ppm), and the slowly relaxing narrow orthorhombic crystalline phase ($\delta = 32.8$ ppm). The 10 s $T_{1,C}$-filtered CP/MAS spectrum, Fig. 1(d), selectively retains the orthorhombic and monoclinic ($\delta = 34.2$ ppm) crystalline components, allowing deconvolution of the relative areas. The absolute abundances of the crystalline phases for each sample, shown in Table 1, were determined from the spectra by the previously reported procedure [15]. The method involves subtraction of the 10 s DP/MAS spectrum from the 2000 s spectrum to calculate the area of the crystalline phase. Corrections are incorporated into the calculation to account for incomplete relaxation after 2000 s, partial decay of crystalline magnetization after 10 s, and loss of signal due to spinning sidebands. The results show that the thermodynamically unstable monoclinic phase disappears during annealing, a phenomenon previously reported for polyethylene [44]. The orthorhombic phase also decreased by 3%, a result consistent with the DSC results [1].

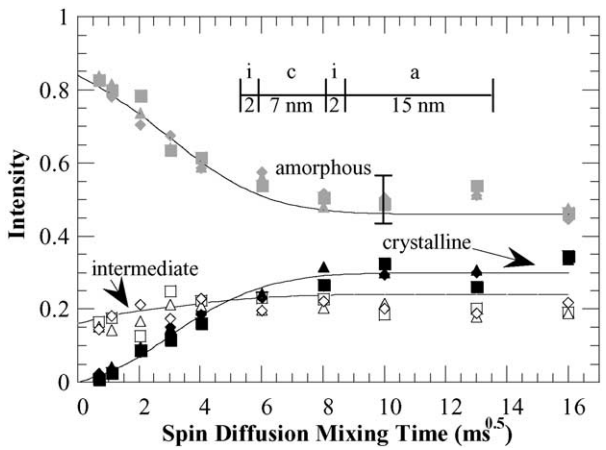

Fig. 2. ^{1}H spin diffusion NMR experiments with ^{13}C detection for (■) unaged, (▲) irradiated, and (▼) annealed. The simulated build-up curves assume a 26 nm repeat length (7 nm crystalline, 2 nm intermediate, and 15 nm amorphous regions).

Table 1
Relative abundance, relaxation constants, linewidths, and chemical shifts of amorphous, intermediate, orthorhombic crystalline, and monoclinic crystalline components in unaged, irradiated, and irradiated + annealed XLPO cable insulation. The amorphous and intermediate components were determined using DECRA analysis while the orthorhombic and monoclinic components were determined from ^{13}C DP/MAS and $T_{1,C}$-filtered CP/MAS experiments. The $T_{1,C}$ values for the orthorhombic component are slopes not relaxation rates

Component	%	$T_{1,C}$ (s)	FWHM (Hz)	δ (ppm)
Amorph. (unaged)	45 ± 5	0.37 ± 0.03	135 ± 5	30.8
Amorph. (irradiated)	49 ± 5	0.39 ± 0.03	161 ± 5	30.7
Amorph. (annealed)	54 ± 5	0.39 ± 0.03	137 ± 5	30.7
Interm. (unaged)	23 ± 5	1.43 ± 0.3	71 ± 5	32.9
Interm. (irradiated)	19 ± 5	1.75 ± 0.3	64 ± 5	32.9
Interm. (annealed)	18 ± 5	2.10 ± 0.3	62 ± 5	32.9
Ortho. (unaged)	31 ± 3	16.7 ± 1.5 $s^{-0.5}$	25 ± 3	32.8
Ortho. (irradiated)	31 ± 3	12.8 ± 0.6 $s^{-0.5}$	28 ± 3	32.8
Ortho. (annealed)	28 ± 3	12.3 ± 0.4 $s^{-0.5}$	27 ± 3	32.8
Mono. (unaged)	0.6 ± 0.2	–	–	34.2
Mono. (irradiated)	0.6 ± 0.2	–	–	34.2
Mono. (annealed)	<0.1	–	–	–

3.2. Determination of domain size

^{1}H spin diffusion experiments with ^{13}C detection via CP probed the crystalline lamellar thickness in the samples. The experiments observed similar build-up curves for the unaged, irradiated, and irradiated + annealed samples. The data is shown in Fig. 2 and simulated using the Euler method assuming diffusion coefficients estimated by ^{1}H T_2^{-1} constants [39] to be 0.8, 0.7, and 0.4 nm^2/ms for the crystalline, intermediate, and amorphous phases, respectively. The simulations determined that the average total repeat length was 26 ± 13 nm. Assuming densities of 1.000 and 0.855 g/mol for the crystalline and amorphous phases,

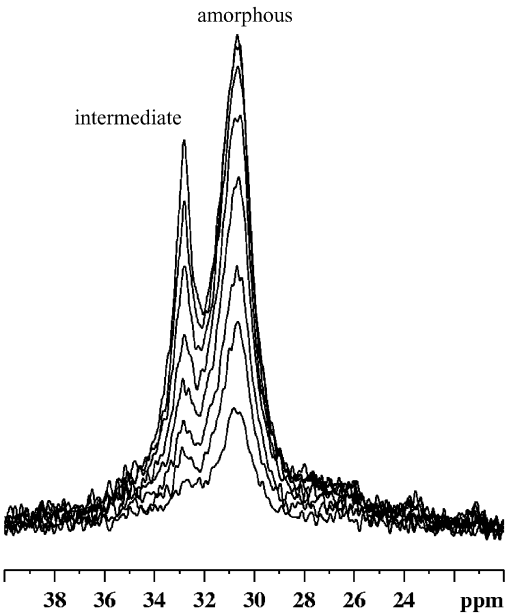

Fig. 3. ^{13}C DP/MAS spectra of irradiated XLPO cable insulation. The effective recycle delays are 0.1, 0.2, 0.3, 0.5, 0.8, 1.3, 2, and 3 s. The amorphous component is observable on the right and the intermediate component is the slower relaxing component on the left.

respectively [45,46], the thickness of the crystalline regions is approximately 7 ± 4 nm. The intermediate components are estimated to be 2 ± 1 nm. The relative dimensional layout is schematically shown as an insert in Fig. 2. The large relative error margins are due to uncertainty in shape and spin diffusion coefficients of the amorphous and intermediate phases. Regardless of the large absolute uncertainty of dimensions, the similar shapes of the curves show that the three materials all have similar domain sizes. The broad melting peaks observed in DSC [1] suggest a broad distribution of lamellar thickness, but the spin diffusion experiments are not sufficiently precise to quantify the distribution.

3.3. Analysis of amorphous and intermediate domains

Chemometric analysis of the 30 ^{13}C DP/MAS spectra obtained using different delay times for each sample revealed modest changes in component concentrations and relaxation constants. The signal-to-noise ratios in the DP/MAS spectra were adequate for the DECRA method, ranging from 25:1 for the 0.1 s effective recycle delay experiment to 80:1 for the 3 s experiment. Selected spectra of the irradiated sample are shown in Fig. 3. The intermediate and amorphous components are both identifiable, although neither is completely resolved. The amorphous phase ($\delta = 30.7$ ppm) has faster dynamics and thus is almost fully relaxed after 1.3 s. The highly *trans* intermediate component has a slower relaxation constant and an isotropic chemical shift of $\delta = 32.9$ ppm, slightly downfield from the crystalline peak at 32.8 ppm. Branches, side chains, crosslinks, and comonomers result in additional

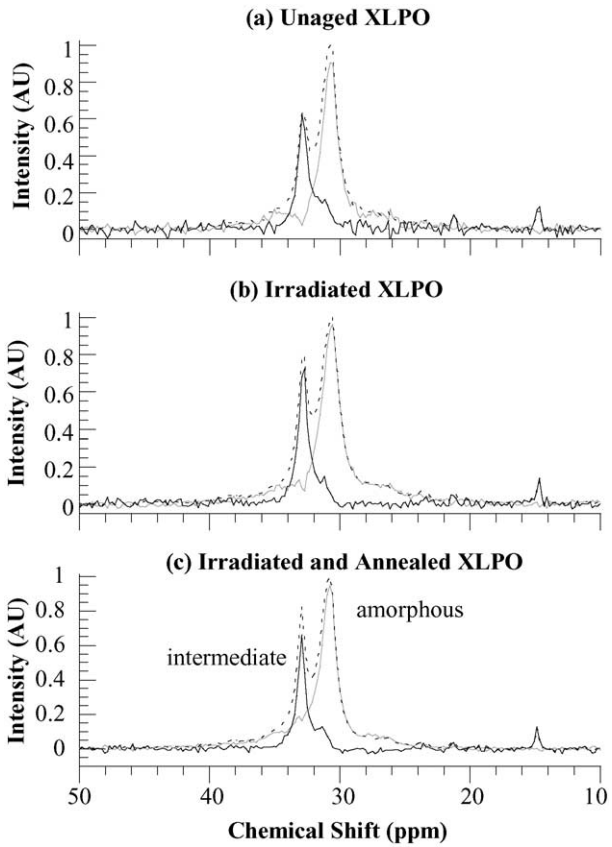

Fig. 4. The DECRA determined lineshapes of the intermediate and amorphous components in unaged, irradiated and irradiated + annealed XLPO samples. The dashed lines show the sum of the components. The spectra are scaled to equal maximum intensity.

resonances that have chemical shifts ranging between $\delta =$ 38 ppm for tertiary carbons and $\delta = 14$ ppm for methyl groups [47]. Some of the peaks arising from the chemically inequivalent carbons are expected to overlap the intermediate and amorphous polyethylene peaks.

Despite the minor peaks, the DECRA chemometric analyses were successfully applied to resolve the intermediate and amorphous phases. The only adjustable parameter used in the DECRA program was the number of components, defined to be 3 to account for the two phases and the addition of the 'constant' component that created the proportionality condition (see Section 2). Setting the number of components to a higher value only yielded noise in the recovered pure component spectra. The resulting resolved amorphous and intermediate lineshapes for each sample are shown in Fig. 4.

The linewidth of the intermediate component shows slight narrowing from 71 to 64 Hz upon irradiation, but no further change after subsequent annealing. The linewidth of the amorphous peak also undergoes a slight modification during irradiation, increasing from 135 to 161 Hz. The width returns to 137 Hz after annealing. The linewidth of the intermediate component may be related to modified dynamics after irradiation. This hypothesis is supported by

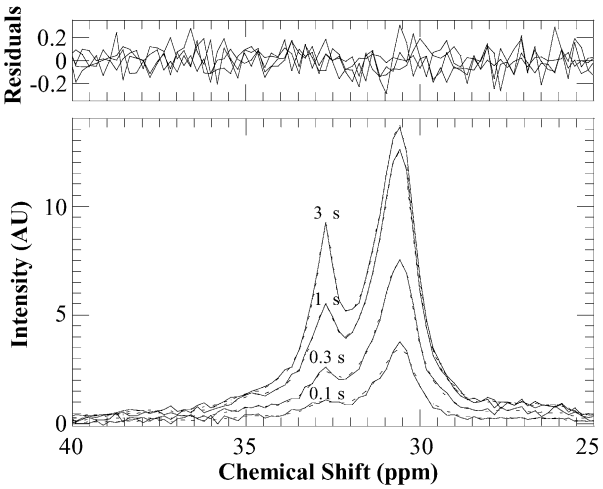

Fig. 5. Experimental (solid lines) and chemometric (dashed) ^{13}C DP/MAS spectra of irradiated + annealed XLPO cable insulation. The effective recycle delay for the spectra are 0.1, 0.3, 1, and 3 s. The differences between the recreated and experimental data are shown in the upper plot. The scale is adjusted by a factor of 5 to more clearly resolve the residuals.

the longer $T_{1,C}$ relaxation constants discussed later in this work. The conformation of the intermediate phase is assumed on the basis of chemical shift to be highly *trans* but some bonds must be in the *gauche* conformation. Changes in conformation statistics could also be partially responsible for linewidth differences but this was not further investigated. Both dynamics and conformation also affect the amorphous lineshape. We did not try to resolve the origin of the small changes observed in the amorphous signal. Future work may reveal if the linewidth of the amorphous phase can be related to elongation but we cannot justify any correlation with the limited data.

The methyl signal at ~15 ppm is assigned by the DECRA algorithm to the intermediate phase. This assignment shows that the $T_{1,C}$ relaxation constant of the methyl groups are similar to that of the intermediate component. However, this observation does not suggest that the methyl groups are in the intermediate phase. The faster dynamics of the methyl groups are expected to result in a longer $T_{1,C}$ relaxation constant. Exchange NMR techniques could be used to confirm this.

Multiplying the resolved components by the recovered concentration profiles reconstructed the 30 spectra for each sample. Fig. 5 shows four of the experimental and reconstructed spectra for the irradiated + annealed XLPO sample. The residuals for all spectra are small and suggest that the lineshapes of the components are invariant with the relaxation times used in this study. This observation is not trivial. Gradients in dynamics within the phases could create multiple lineshapes with different relaxation constants and would result in significant residuals. These gradients were not observed in this study.

In addition to determining lineshapes, the DECRA analysis revealed the relaxation behavior and concentrations for each phase. The recovered concentration profiles are

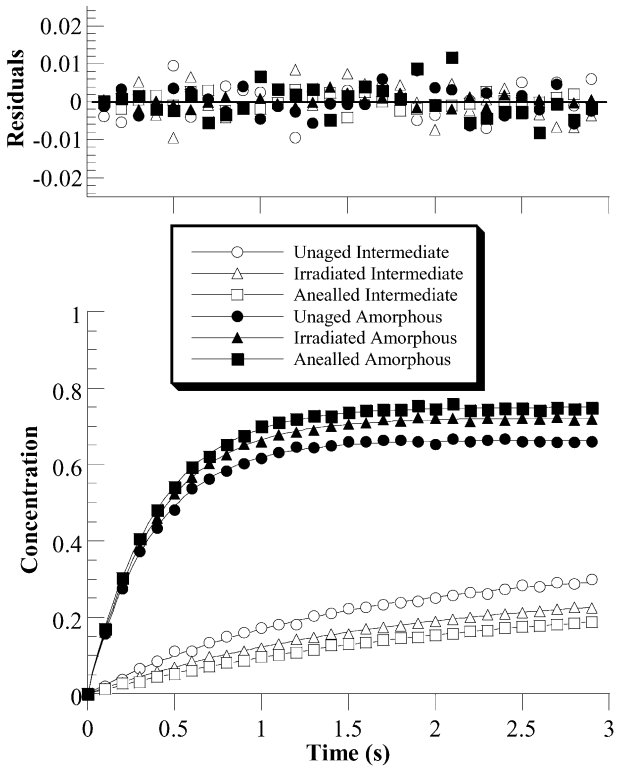

Fig. 6. Relative concentrations of intermediate and amorphous components in XLPO samples obtained from chemometrics. Best-fit curves assuming exponential relaxation are shown using parameters listed in Table 1. Residuals are expanded by a factor of 10 to show the unpatterned behavior.

shown in Fig. 6. Exponential curve-fits for each sample are plotted in the figure and the estimated abundances and relaxation constants are listed in Table 1. The difference between the best-fits and the experimental results do not show significant or patterned deviations from exponential behavior. As discussed later, the residual concentration curve is sensitive to non-exponential behavior and the expanded *y*-axis in the plot facilitates visual detection.

Several differences between the samples were elucidated. The amorphous phase concentration is less in the unaged sample (66% of non-crystalline area, i.e. the amorphous + intermediate components) than in either the irradiated (71%) or annealed samples (75%). However, the uncertainty of these values is large and the variation may not be statistically significant. A visual inspection of Fig. 4 suggests that inconsistencies in the deconvoluted lineshapes might overwhelm any real changes in the concentration of the components. One example of this uncertainty arising from unequal lineshapes is the greater intensity of the intermediate peak observed in the irradiated spectra compared with the unaged sample, but a lower deconvoluted concentration. We therefore have listed generous error margins in Table 1.

The apparent relaxation constants for the intermediate phase becomes slower after irradiation and even slower after annealing ($T_{1,C} = 1.43$, 1.75, and 2.10 ± 0.3 s for the unaged, irradiated, and irradiated + annealed, respectively).

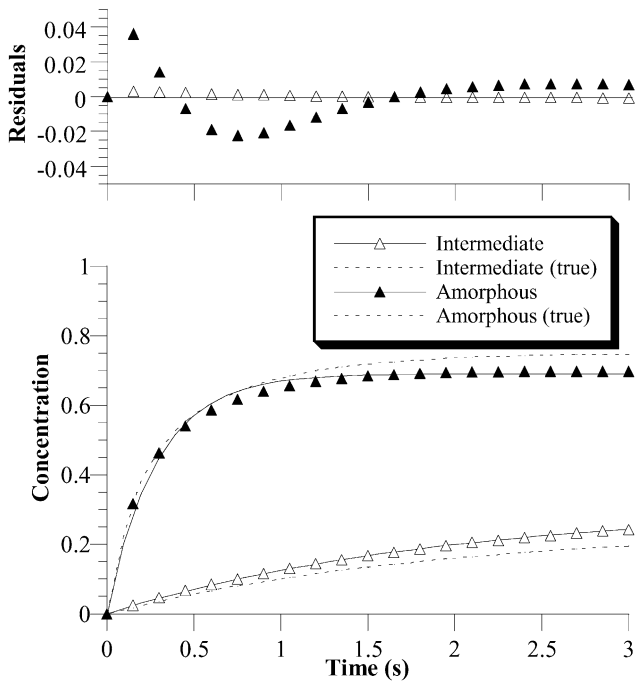

Fig. 7. Example of DECRA analysis on multi-exponential data. The synthetic data was created assuming that the system is comprised of an amorphous signal (37.5%, $T_{1,C} = 0.15$ s; 37.5%, $T_{1,C} = 0.6$ s) and an intermediate component (25%, $T_{1,C} = 1.95$ s) The true data set is shown by the dashed lines and has significant deviations from the reconstructed intensities (triangles). Patterned residuals exist in the upper plot with a scale expanded by a factor of 5.

The longer $T_{1,C}$ relaxation constants observed after irradiation suggests that the narrower linewidth observed for the intermediate component is due to modified dynamics. The relaxation values obtained for the intermediate component are all faster than the 6–8 s $T_{1,C}$ relaxation constants reported in a previous study that examined irradiated highly crystalline (77%) polyethylene [48]. However, the results determined in those previous studies used a bi-exponential fit to the 32.8 ppm peak intensity, a method likely to be erroneous because of treatment of the recovery in the crystalline phase as a traditional exponential process. Chemometrics provides an excellent technique for determining relaxation constants of the intermediate component because the analysis simultaneously determines both lineshape and recycle time dependence of the signal.

The trends of $T_{1,C}$ relaxation constants shown in this work are surprising and cannot explain the changes of mechanical properties. The irradiated + annealed sample ($e = 220\%$) has an ultimate elongation value similar to that of the unaged material ($e = 310\%$) yet has the longest intermediate relaxation constant. The extent of oxidation, approximately 1 wt% O_2, may affect the dynamics of the phases, but the changes could also be due to crosslinking. We are uncertain of the relationships between morphology and dynamics of undrawn materials and the changes that occur during mechanical deformation. Currently work is being performed to study the effects of elongation on the morphology of polyethylene [23], but these results have not been applied to XLPO cable insulation.

One concern arising during the DECRA analysis is the ability to identify non-exponential or multi-exponential relaxation behavior. The chemometric method attempts to resolve components on the basis of exponential decay constants, but is capable of extracting the true relaxation profile in a complex system if there is a significant distinction between the short components and long components. To demonstrate this principle, a synthetic multi-exponential data set was constructed containing equal concentrations of amorphous components with relaxation constants of 0.15 and 0.6 s, and an intermediate component with a relaxation constant of 1.95 s. The analyzed concentrations are shown in Fig. 7 and show a significant deviation from the original data set. A fraction of the slower relaxing amorphous phase was assigned to be in the intermediate component and the intermediate component lineshape has intensity in the amorphous region. Nevertheless, deviation from a mono-exponential behavior was discernible by the patterned residuals. The maximum residual value in the test was 0.04 while experimental residuals in the XLPO study were less than 0.01. Note that the expansion factor in the residual graph of Fig. 6 is twice the value used in Fig. 7. The lack of significant residual intensity in the experimental data proves that the dynamics in the amorphous phase is relatively homogenous on the time scale of the $T_{1,C}$ relaxation constant, 0.4 s.

3.4. Determination of crystalline dynamics

The final aspect explored by this work was the effect of helical jumps. In uncrosslinked polyethylene, helical jumps of the crystalline chains have been shown to transport atoms into the fast-relaxing intermediate and amorphous domains [36,49]. The $T_{1,C}$ relaxation process for the crystalline domains has been suggested to be diffusion limited, and the helical jump rate is related to the slope of the crystalline intensity plotted versus $\sqrt{t}$ where t is the recycle delay. The phenomenon has also been detected in crosslinked polyethylene, albeit at a slower rate (~45% lower diffusion coefficient) [48,50]. The results of the DECRA analyses for the intermediate phase and $T_{1,C}$-filtered CP/MAS experiments obtained in this work for the XLPO samples were used to plot the combined crystalline and intermediate concentrations versus the square root of the recycle/$T_{1,C}$-filter delay, Fig. 8. Similar relaxation curves were seen for all three samples; an abrupt change of slope occurs near 4 s when the intermediate phase is almost fully relaxed. The loss of magnetization in the slow relaxation region for the unaged material has a lower slope ($0.060 \pm 0.005\ s^{-0.5}$) than observed for the other two samples ($0.080 \pm 0.003\ s^{-0.5}$). Those normalized values were determined by dividing the observed slopes by the

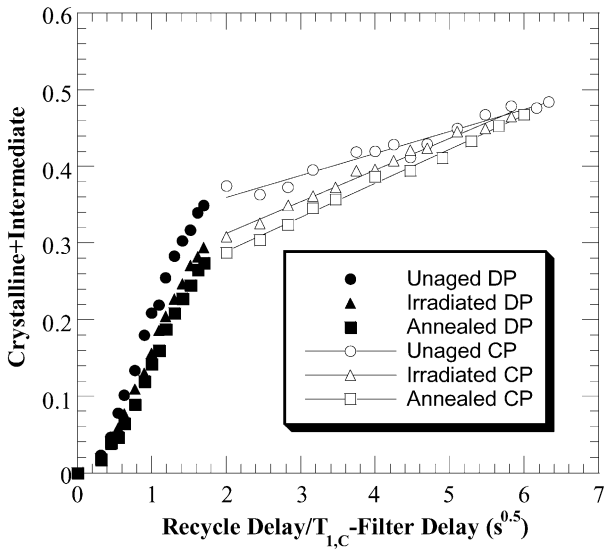

Fig. 8. Fractional recovery of the intermediate and crystalline components versus $\sqrt{t}$. A value of 1 corresponds to complete recovery of both phases. The data was obtained from the chemometric analyses of the DP spectra (solid symbols) and integration of $T_{1,C}$-filtered CP/MAS experiments (hollow symbols). The data from the CP/MAS experiments were forced to intercept the DP curve.

relative concentrations of the crystalline phase. Although not truly relaxation constants, the reciprocals of these slopes are listed in the $T_{1,C}$ column for the orthorhombic crystalline components in Table 1.

The diffusion coefficient can be related to the decay of crystalline magnetization in $T_{1,C}$-filtered CP experiments using the following equation

$$D = d_c^2 \pi / 16 \varepsilon^2 t_m^s \tag{14}$$

where d_c is the crystalline thickness, ε is the dimensionality (1 for lamellae), and t_m^s is the intercept with the time axis when a straight line is draw through the points in a $I_C(\sqrt{T_{1,C}} - \text{filterdelay})$ graph. The points used to draw this line must be for times after the decay of the intermediate and amorphous components. Eq. (14) differs from the equations typically used to calculate the lamellar thickness from the initial slope in a spin diffusion experiment [36] because the rate of magnetization decay in the intermediate phase is faster than the diffusion rate. The assumption used to derive Eq. (14) requires that

$$\frac{\sqrt{T_{1,C}(\text{Intermediate})}}{A_i} \ll \frac{\sqrt{t_m^s}}{A_c} \tag{15}$$

where A_i and A_c are the relative abundances of the intermediate and crystalline phases. This inequality fails at higher temperatures.

Using Eq. (14), the physical diffusion coefficients of CH_2 units in the crystalline domain are estimated to be 0.03 nm^2/s for the unaged sample and 0.06 nm^2/s for the irradiated and irradiated + annealed samples. These values are much smaller than the ^1H spin diffusion coefficient used to calculate lamellar thickness, 0.8 nm^2/s. At higher temperatures or in other materials, the physical diffusion may become faster than ^1H spin diffusion. In such circumstances, lamellar thickness could not be determined.

The physical diffusion coefficient can be converted into a jump rate by dividing the square of the *c*-axis distance per CH_2 unit, 0.0163 nm^2 [51]; the jump rates are 2 s^{-1} for the unaged material and 4 s^{-1} for the irradiated and irradiated + annealed samples. The absolute uncertainty of these values is high due to the large error margin for the lamellar length, but the relative uncertainty of the ratio of the coefficients is much smaller. The numbers obtained in this work are similar to values extrapolated from jump rates in ultra-high molecular weight polyethylene [49].

There is a fortuitously large difference in slope between the intermediate and crystalline relaxation regimes. Only a small amount of magnetization will be transferred to the crystalline domains during experiments with recycle delays less than 3 s. Larger transfer rates would require complicated simulations to extract the true intermediate component and also would make the apparent relaxation constant deceptively large. We urge caution to readers who attempt to extract the intermediate component concentration, relaxation constants, and crystalline jump rates in systems where no abrupt change of slope is observed in the relaxation curve. Inappropriate analysis of data may have lead to the current discrepancy for activation energy of chain diffusion [48–50].

An interesting conclusion, although not particularly germane to explaining the Lazarus effect, can be derived from the observed relaxation behavior in this system. At ambient temperatures, the magnetization is transferred from the intermediate phase into the crystalline phase. Previous Monte Carlo simulations of the helical jumps [49] and NOE measurements [48] suggested that the magnetization originates in the amorphous domains and then is transferred by the chain diffusion into the intermediate and crystalline regions. Those results were obtained at elevated temperatures (60–104 °C) where the helical jump rates are several orders of magnitude higher than at ambient temperatures. At such high jump rates, physical diffusion of amorphous chains may indeed relax the intermediate phase. If such a process had dominated relaxation in this system at ambient temperatures, the intermediate component would have had a slope similar to the crystalline intensity when plotted versus $\sqrt{t}$.

4. Conclusions

The chemometric DECRA algorithm is a powerful tool to enhance solid-state NMR analysis of polyolefin morphology and dynamics. No assumption of lineshape or relaxation constants is necessary to conduct the analysis. The analysis resolved the intermediate and amorphous

lineshapes and concentration profiles for XLPO samples. The fits of the relaxation curves showed no deviation from a mono-exponential behavior for either the amorphous or intermediate components, suggesting dynamic homogeneity in these regions. The dynamics of the intermediate phase, implied by the measured lineshapes and $T_{1,C}$ relaxation constants, slowed after irradiation and then further decreased after annealing. These observations leave many unanswered questions about the role of the intermediate phase in semicrystalline polymer deformation. Current work is being pursued to apply chemometrics to determine the nature of the intermediate component in a more experimentally ideal semicrystalline polymer, high-density polyethylene.

Acknowledgments

Sandia is a multi-program laboratory operated by Sandia Corporation, a Lockheed Martin Company, for the United States Department of Energy under Contract DE-AC04-94AL8500.

References

[1] Celina M, Gillen KT, Wise J, Clough RL. Radiat Phys Chem 1996;48: 613–26.
[2] Celina M, Gillen KT, Clough RL. Polym Degrad Stab 1998;61:231.
[3] Popli R, Mandelkern L. J Polym Sci: Polym Phys 1987;25:441.
[4] Mandelkern L. Polym J 1985;17:337.
[5] O'Donnell JA, Whittaker AK. JMS Appl Pure Chem 1992;A29(1):1.
[6] Torikai A, Geetha R, Nagaya S, Fueki K. J Polym Sci 1990;28:3639.
[7] Earl WL, VanderHart DL. Macromolecules 1979;12:762.
[8] VanderHart DL, Khoury F. Polymer 1984;25:1589.
[9] Tonelli AE, Schilling FC. Acc Chem Res 1981;14:233.
[10] Aoki A, Asakura T. In: Ando I, Asakura T, editors. Solid state NMR of polymers. Studies in physical and theoretical chemistry, vol. 84. Amsterdam: Elsevier; 1998. p. 415.
[11] Yamanobe T. In: Ando I, Asakura T, editors. Solid state NMR of polymers. Studies in physical and theoretical chemistry, vol. 84. Amsterdam: Elsevier; 1998. p. 267.
[12] Mandelkern L. Acc Chem Res 1990;23:380.
[13] Mandelkern L. Chemtracts: Macromol Chem 1992;3:347.
[14] Mutter R, Stille W, Strobl GR. J Polym Sci, Polym Phys Ed 1993;31: 99.
[15] Hu W-G, Schmidt-Rohr K. Polymer 2000;41:2979–87.
[16] Kitamaru R, Horii F. Adv Polym Sci 1978;26:138.
[17] Smith JB, Manuel AJ, Ward IM. Polymer 1975;16:57.
[18] Kuwabara K, Kaji H, Horii F, Bassett DC, Olley RH. Macromolecules 1997;30:7516.
[19] Eckman RR, Henrichs PM, Peacock AJ. Macromolecules 1997;30: 2474.
[20] Cheng J, Fone M, Reddy VN, Schwartz KB, Fisher HB, Wunderlich B. J Polym Sci, Polym Phys Ed 1994;22:589.
[21] Kitamaru R, Horii F, Murayama K. Macromolecules 1986;19:636.
[22] Harris DJ, Tischendorf B, Alam TM. To be published.
[23] Mowery DM, Harris DJ, Schmidt-Rohr K. To be published.
[24] Alam TM, Alam MK. Spectroscopy 2001;16:18.
[25] Belton PS, Colquhoun IJ, Kemsley EK, Delgadillo I, Roma P, Dennis MJ, Sharman M, Holmes E, Nicholson JK, Spraul M. Food Chem 1998;61:207–13.
[26] Vlahov G, Shaw AD, Kell DB. J Am Oil Chem Soc 1999;76:1223.
[27] Sacco A, Brescia MA, Liuzzi V, Reniero F, Guillou C, Ghelli S, vanderMeer P. J Am Oil Chem Soc 2000;77:619.
[28] Wickholm K, Larsson PT, Iverson T. Carbohydr Res 1998;312:123.
[29] Wallbäcks L, Edlund U, Nordèn B. J Wood Chem Tech 1989;9:235.
[30] Shaw AD, diCamillo A, Vlahov G, Jones A, Bianchi G, Rowland J, Kell DB. Anal Chim Acta 1997;348:357.
[31] Alam MK, Alam TM. Spectrochem Acta, Part A 2000;56:729.
[32] Malkavaara P, Alen R, Kolehmainen E. Magn Reson Chem 1999;37: 407.
[33] Sylvestre EA, Lawton WH, Maggio MS. Technometrics 1974;16:353.
[34] Stilbs P, Paulsen K, Griffiths PC. J Phys Chem 1996;100:8180.
[35] Stilbs P, Paulsen K. Rev Sci Instrum 1996;67:4380.
[36] Schmidt-Rohr K, Spiess HW. Multidimensional solid-state NMR and polymers. San Diego: Academic Press; 1994.
[37] Torchia DA. J Magn Reson 1978;30:613.
[38] Bennett AE, Rienstra CM, Auger M, Lakshmi KV, Griffin RG. J Chem Phys 1995;103:6951.
[39] Mellinger F, Wilhelm M, Spiess HW. Macromolecules 1999;32:4686.
[40] VanderHart DL, McFadden GB. Solid State Nucl Magn Reson 1996; 45.
[41] VanderHart DL. Makromol Chem Macromol Symp 1990;34:125.
[42] Packer KJ, Pope JM, Yeung RR, Cudby MEA. J Polym Sci, Polym Phys Ed 1984;22:589.
[43] Windig W, Antalek B. Chemom Intell Lab Syst 1997;37:241.
[44] Russell KE, Hunter BK, Heyding RD. Polymer 1997;38:1409.
[45] Kitamaru R, Mandelkern L. J Polym Sci 1970;8:2079.
[46] Chiang R, Flory PJ. J Am Chem Soc 1961;83:2857.
[47] Brandolini AJ, Hills DD. NMR spectra of polymers and polymer additives. New York: Marcel Dekker; 2000.
[48] Robertson MB, Ward IM, Klein PG, Packer KJ. Macromolecules 1997;30:6893.
[49] Schmidt-Rohr K, Spiess HW. Macromolecules 1991;24:5288.
[50] Klein PG, Robertson MB, Driver MAN, Ward IM, Packer KJ. Polym Int 1998;47:76.
[51] Bunn CW. Trans Faraday Soc 1939;35:482.